

Resonant state selection in synthetic ferrimagnets

B. C. Koop,¹ Yu. I. Dzhezherya,² K. Demishev,² V. Yurchuk,² D. C. Worledge,³ and V. Korenivski^{1,*}

¹*Royal Institute of Technology, 10691 Stockholm, Sweden*

²*Institute of Magnetism, Ukrainian Academy of Sciences, Kiev, Ukraine*

³*IBM T. J. Watson Research Center, Yorktown Heights, NY 10598, USA*

(Dated: June 13, 2022)

Resonant activation of a synthetic antiferromagnet (SAF) is known to result in a dynamic running state, where the SAF's symmetric spin-flop pair continuously rotates between the two antiparallel ground states of the system, with the two magnetic moments in-phase in the so-called acoustical spin-resonance mode. The symmetry of an ideal SAF does not allow, however, to deterministically select a particular ground state using a resonant excitation. In this work, we study asymmetric SAF's, or synthetic ferrimagnets (SFi), in which the two magnetic particles are different in thickness or are biased asymmetrically with an external field. We show how the magnetic phase space of the system can be reversibly tuned, post-fabrication, between the antiferro- and ferri-magnetic behavior by exploiting these two asymmetry parameters and applying a uniform external field. We observe a splitting of the optical spin-resonance for the two ground states of the SFi system, with a frequency spacing that can be controlled by a quasistatic uniform external field. We demonstrate how the tunable magnetic asymmetry in SFi allows to deterministically select a particular ground state using the splitting of the optical spin-resonance. These results offer a new way of controlling the magnetic state of a spin-flop bilayer, currently used in such large scale applications as magnetic memory.

PACS numbers:

I. INTRODUCTION

Magnetic memory technology employs the effects giant magnetoresistance^{1,2} and tunneling magnetoresistance^{3,4} in spin-valves type sensors⁵. In these, the switching of the magnetic state is achieved by using either external magnetic field⁶⁻⁹ or spin-transfer-torque¹⁰⁻¹³ writing. In this work we demonstrate a reliable way to switch a magnetic nanodevice employing microwave excitation in resonance with the spin eigen-modes in the device, which act to amplify the action of the microwave field.

Synthetic antiferromagnets consist of two identical dipole-coupled magnetic layers separated by a thin spacer. The dipole coupling results in an antiparallel (AP) alignment of the magnetic moments in the ground state, which makes them similar to classical atomic antiferromagnets but with a tunable coupling strength between the magnetic moments set in fabrication by a suitable choice of the material parameters and geometry. When the lateral shape is elliptical, the system has two AP ground states, in which the moments are aligned along the easy-axis (EA) of the ellipse. Due to the symmetry, the energy of the two AP ground states is degenerate.

The quasistatic¹⁴⁻¹⁶ and dynamic¹⁷⁻²⁰ behavior of SAFs has been studied extensively. Due to the nearly perfect flux closure in the AP state, SAFs are characterized by high stability against thermal agitation²¹. It was recently shown that the spin dynamics contains collective acoustical and optical resonance modes²². It has also been shown that excitation at the optical resonance frequency can result in switching between the two AP ground states²³, typically resulting in multiple switching

or a spin-running state, since the resonant switching in an ideal SAF is symmetric for the two AP ground states so a specific state cannot be selected deterministically.

In order to enable use of resonant excitation for selecting a specific ground state, which is highly desirable for applications, the spin-resonance spectrum can be tuned such that, for example, resonant switching occurs at different frequencies for the two ground states. For this the spin-flop bilayer must have suitable magnetic asymmetry, such as asymmetry in the the magnitude of the two magnetic moments or asymmetric field biasing of the layers externally so each layer experiences a different Zeeman field. The former can be achieved by making the two layers of the same material but slightly different thickness or of the same thickness but of materials with different saturation magnetization. The latter can be built-in into the nominally flux-closed reference layer of the read out junction²⁴. These two magnetic asymmetry contributions can also be combined, which we do in this study for achieving greater flexibility in controlling the energetics and spin dynamics in the SFi system.

In this paper we develop a method of deducing the individual magnetic asymmetry contributions in SFi, post-fabrication, and show how they can be used to reversibly tune the magnetic behavior of the system between SAF-like and SFi-like. We further show how an external uniform magnetic field can be used to control the symmetry of the magnetic double-well potential as well as the splitting of the optical spin resonance in SFi with a thickness imbalance and asymmetric local field-bias.

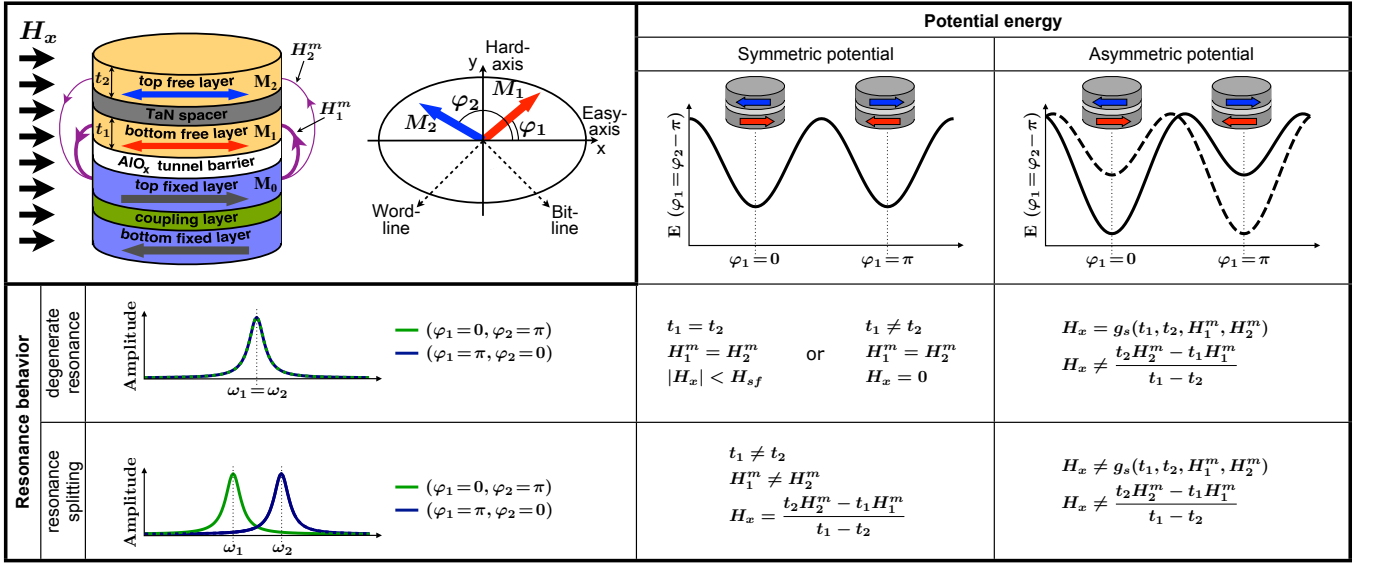


FIG. 1: (Color online) The top-left panel illustrates the layout of the nanopillar, which integrates an SFi bilayer and a nearly flux-closed read-out layer, separated by an Al-O tunnel junction, subject to a quasistatic magnetic field H_x directed along the easy axis; the top-view schematic shows the magnetic layout of the bilayer, with the two dipole-coupled moments at angles φ_1 and φ_2 . The optical spin resonance for the two ground states is illustrated in the bottom-left panel for a symmetric bilayer (SAF; single resonance peak) and an asymmetric bilayer (SFi; resonance doublet). The magnetic asymmetry is achieved by a thickness imbalance ($t_1 \neq t_2$) and/or asymmetric fringing field from the reference layer acting on the individual layers in the spin-flop bilayer ($H_1^m \neq H_2^m$). The top-right panels illustrate the symmetric and asymmetric magnetic potentials, generally corresponding to SAF and SFi. Interestingly, as shown in detail analytically in the text below, suitable magnetic asymmetry combined with a uniform external biasing field (H_x) can be used to reversibly tune the system between SAF-like (symmetric potential minima and a single resonance) and SFi-like (asymmetric potential and a resonance doublet) behavior. $H_x = H_{sf}$ is the spin-flop field of the bilayer, at which one of the minima vanishes completely and the two macrospins switch into a scissor state. The degeneracy in the magnetic potential and the sign and magnitude of the resonance splitting depend on the sign and magnitude of the external uniform biasing field (see text for details), which provides an easy and powerful tool for mapping out and controlling the static and dynamic properties of the system.

II. SFI EIGEN-MODES

In this section we develop specific predictions for spin dynamics in SFi, which are then used to guide the experiment. In particular, we find analytically that the optical spin resonance in the system splits into a doublet, which allows controlled selection of the individual ground states using resonant microwave pulses modulated in frequency. We start by illustrating in Fig. 1 the energetics of SFi, including the key symmetry criteria for SAF-like versus SFi-like magnetic behavior.

In the macrospin approximation, appropriate for our sub-micrometer junctions, with the z-axis out-of-plane and the in-plane easy-axis (EA) due to shape anisotropy along x , the total magnetic energy (E) of the bilayer can be written as¹⁶

$$\frac{E}{2\pi M_S^2} = \sum_{i,j=1;i \neq j}^2 V_i \{ N_{ix} m_{ix}^2 + (N_{iy} + h_u) m_{iy}^2 + N_{iz} m_{iz}^2 + \gamma_{jx} m_{1x} m_{2x} + \gamma_{jy} m_{1y} m_{2y} + \gamma_{jz} m_{1z} m_{2z} \} - 2(h_x + h_{ix}^m) m_{ix} - 2h_y \cos(\omega t) m_{iy}, \quad (1)$$

where M_S is the saturation magnetization of the material (here taken to be same in both layers); $V_i = \pi a b t_i / 4$ the

volume of layer i with a , b and t_i the length, width, and thickness of that layer, respectively; $N_{i\alpha}$ the demagnetizing factor of layer i in the α -direction, with $\sum_{\alpha} N_{i\alpha} = 1$ and $N_{i\{x,y\}} = n_{\{x,y\}} t_i / b$, and $n_{\{x,y\}}$ the reduced demagnetizing factors²⁵; \mathbf{m}_i the cartesian unit magnetization vector of the i -th layer; $h_u = H_u / 4\pi M_S$ the normalized intrinsic uniaxial anisotropy field along the easy-axis; $h_y = H_y / 4\pi M_S$ the normalized amplitude of the applied microwave field in the y -direction; ω the frequency of the microwave field; $h_x = H_x / 4\pi M_S$ the normalized external quasistatic easy-axis field; $h_i^m = H_i^m / 4\pi M_S$ the normalized asymmetric biasing field (fringing field) acting on layer i in the x -direction; $\gamma_{i\alpha} = r_{\alpha} N_{i\alpha}$ the inter-layer exchange field from layer i acting on the other layer in the α -direction²⁶. In our case $\gamma_{i\alpha}$ is solely of dipolar nature. For simplifying the derivation to follow it is convenient to rewrite all terms proportional to t_i through

$$Q_i = [1 - (-1)^i \varepsilon] Q, \quad \varepsilon = (t_1 - t_2) / (t_1 + t_2),$$

such that $Q_i = N_{ix}, N_{iy}, \gamma_{ix}, \gamma_{iy}, V_i$.

The natural coordinate system for SFi is polar, in which

$$\mathbf{m}_i = (\cos \varphi_i \sin \theta_i, \quad \sin \varphi_i \sin \theta_i, \quad \cos \theta_i).$$

For thin magnetic particles elongated in-plane in x , the following holds:

$$N_{ix} < N_{iy} \ll N_{iz} \approx 1; \quad \theta_i = \pi/2 + \xi_i, \quad |\xi_i| \ll 1,$$

and $\cos(\theta_i) \approx -\xi_i$. Quantities r_z, ξ_1, ξ_2 are small parameters in the problem, therefore $\gamma_z \xi_i \xi_j$ can be neglected:

$$\begin{aligned} \frac{W - W_0}{\pi M_S^2} = & - (1 + \varepsilon^2) \left(N_y - N_x + \frac{h_u}{1 + \varepsilon^2} \right) \cos 2\Phi \cos 2\chi + 2\varepsilon \left(N_y - N_x + \frac{h_u}{2} \right) \sin 2\Phi \sin 2\chi \\ & - (1 - \varepsilon^2) [(\gamma_y - \gamma_x) \cos 2\Phi + (\gamma_y + \gamma_x) \cos 2\Phi] - 4(h_x + h_f + \varepsilon h_d) \cos \Phi \cos \chi \\ & + 4[\varepsilon(h_x + h_f) + h_d] \sin \Phi \sin \chi - 4h_y \cos \omega t (\sin \Phi \cos \chi + \varepsilon \cos \Phi \sin \chi) + \frac{1}{2}(m_z^2 + l_z^2 + 2\varepsilon m_z l_z). \end{aligned}$$

Here $W_0 = \pi[(1 + \varepsilon^2)(N_y + N_x) + h_u]M_S^2$; Φ, χ are the normal coordinates and are given by $\Phi = (\varphi_1 + \varphi_2)/2$, $\chi = (\varphi_1 - \varphi_2)/2$; $m_z = \xi_1 + \xi_2$, $l_z = \xi_1 - \xi_2$. Further, the following notations were used: $h_f = (h_1^m + h_2^m)/2$, $h_d = (h_1^m - h_2^m)/2$.

The Lagrange density can now be written as²⁷

$$\begin{aligned} \frac{L}{2\pi M_S^2} = & (1 + m_z) \left(\frac{d\Phi}{d\tau} + \varepsilon \frac{d\chi}{d\tau} \right) \\ & + l_z \left(\frac{d\chi}{d\tau} + \varepsilon \frac{d\Phi}{d\tau} \right) - W(\Phi, \chi, m_z, l_z), \end{aligned}$$

where $\tau = t \cdot \omega_0$, $\omega_0 = 8\pi M_S \mu_B / \hbar$, $\Omega = \omega / \omega_0$. The dynamics of SFi are then described by the following system of equations:

$$\begin{aligned} \frac{d^2}{d\tau^2} (\Phi + \varepsilon\chi) = & h_y \cos \Omega\tau (\cos \Phi \cos \chi - \varepsilon \sin \Phi \sin \chi) - (h_x + h_f + \varepsilon h_d) \sin \Phi \cos \chi - [\varepsilon(h_x + h_f) + h_d] \cos \Phi \sin \chi \\ & - \frac{1}{2} \left\{ [(1 + \varepsilon^2)(N_y - N_x) + h_u] \cos 2\chi + (1 - \varepsilon^2)(\gamma_y - \gamma_x) \right\} \sin 2\Phi - \varepsilon \left(N_y - N_x + \frac{h_u}{2} \right) \cos 2\Phi \sin 2\chi, \\ \frac{d^2}{d\tau^2} (\chi + \varepsilon\Phi) = & h_y \cos \Omega\tau (\varepsilon \cos \Phi \cos \chi - \sin \Phi \sin \chi) - (h_x + h_f + \varepsilon h_d) \cos \Phi \sin \chi - [\varepsilon(h_x + h_f) + h_d] \sin \Phi \cos \chi \\ & - \frac{1}{2} \left\{ [(1 + \varepsilon^2)(N_y - N_x) + h_u] \cos 2\Phi - (1 - \varepsilon^2)(\gamma_y + \gamma_x) \right\} \sin 2\chi - \varepsilon \left(N_y - N_x + \frac{h_u}{2} \right) \sin 2\Phi \cos 2\chi, \end{aligned} \quad (2)$$

These equations naturally yield the two ground states in the absence of microwave field ($h_y = 0$), with $\Phi = \pi/2$, $\chi = \pm\pi/2$, corresponding to the antiferromagnetic vector values of the bilayer $\mathbf{l} = (\pm 2, 0, 0)$.

Solving Eqs. 2 for small oscillations about the two ground states yields the frequencies of the collective spin resonances – the SFi eigen-modes:

$$\begin{aligned} (\Omega^\pm)^2 = & N_y - N_x + \gamma_x + h_u - h_d \sin \chi_0 \pm \left\{ (1 - \varepsilon^2) \gamma_y^2 \right. \\ & \left. + [(h_x + h_f) \sin \chi_0 - \varepsilon(N_y - N_x - \gamma_x)]^2 \right\}^{1/2}. \end{aligned}$$

Here “-” stands for acoustical (in-phase) and “+” for optical (out-of-phase) resonance frequencies (Fig. 2a). The

criterion for generating spin resonance in both ground states, in terms of H_x , is given by

$$\begin{aligned} h_x = & \frac{g_s(t_1, t_2, H_1^m, H_2^m)}{(4\pi M_S)} \\ = & -h_f - h_d \sqrt{1 - \frac{(1 - \varepsilon^2) \gamma_y^2}{h_d^2 - \varepsilon^2 (N_y - N_x - \gamma_x)^2}}. \end{aligned} \quad (3)$$

Here all terms are functions of (t_1, t_2) or (H_1^m, H_2^m) . The optical resonance frequencies for the two ground states are plotted in fig. 2b,c as surfaces in the SFi-asymmetry versus external field parameter space. The bottom plane of figs. 2b,c are intensity plots of the difference in the optical resonance frequency of the two ground

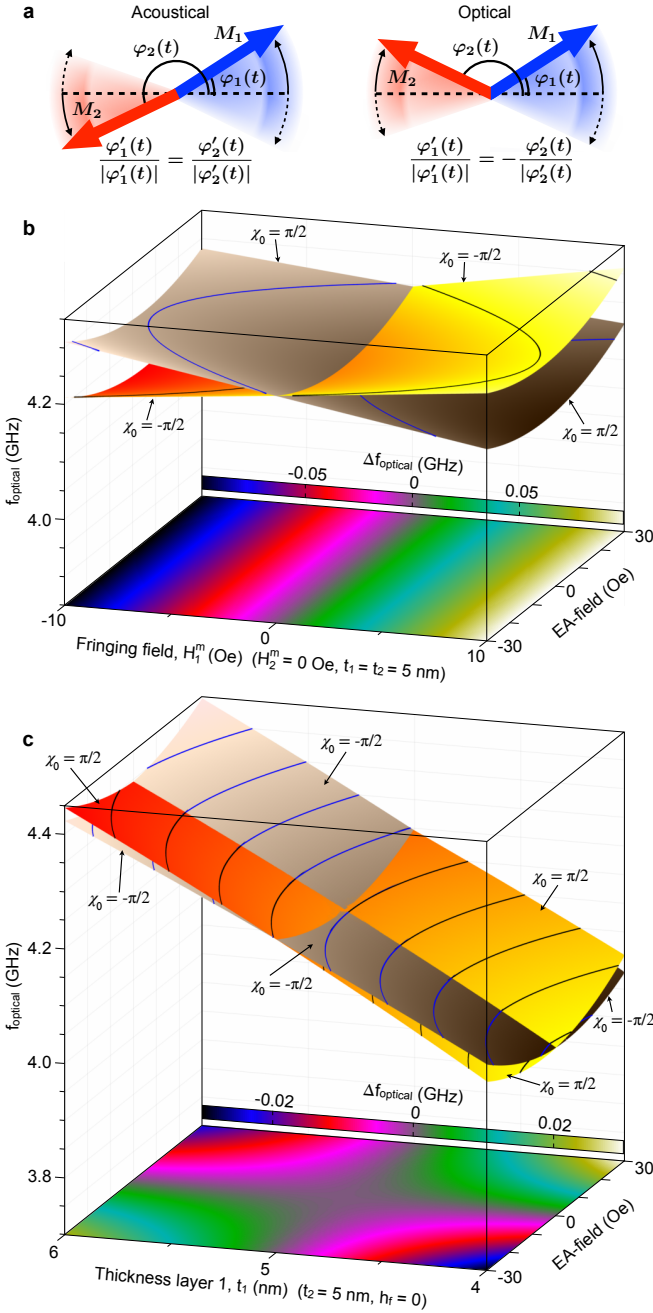


FIG. 2: (Color online) **a**, Schematic of the acoustical (in-phase) and optical (out-of-phase) collective resonance modes; the horizontal dotted line represents the easy-axis; the colored shadows depict the individual macrospin oscillations. **b,c**, The splitting of the optical spin resonance frequency for the two AP states (color scale) as a function of: **b**, H_x and asymmetric biasing (fringing) field, with zero thickness imbalance; **c**, H_x and thickness imbalance, with zero fringing field.

states ($\Delta f_{\text{optical}} = \Delta\Omega^+ \cdot \omega_0/2\pi$), again versus the key asymmetry-field parameters.

In order to determine the mechanism of resonant SFi switching, we next analyze the behavior of the system for

large microwave excitation amplitudes. For this we only consider a fringing field asymmetry (which typically has a stronger effect on the splitting of the optical resonance) and take the thicknesses of the two free layers to be equal ($t_1 = t_2 \Rightarrow \varepsilon = 0$). To simplify the derivations, the external uniform EA-field is set to $h_x = -h_f$, for which the resonance splitting is maximal.

A hard-axis (y -axis) microwave field forces the two macrospins to oscillate out-of-phase, in the optical mode, which results in a modulation of χ . At the same time, Φ only slightly deviates from its ground state of $\Phi_0 = \pi/2$. Therefore, it is a good approximation to take $\varphi = \Phi - \pi/2$ ($|\varphi| \ll 1$). As a result, Eqs. (2) can be rewritten as

$$\frac{d^2\chi}{d\tau^2} + 2\lambda\Omega_o \frac{d\chi}{d\tau} - \Omega_o^2 \sin\chi \cos\chi + h_d \cos\chi + h \cos\Omega\tau \sin\chi = 0. \quad (4)$$

$$\begin{aligned} \frac{d^2\varphi}{d\tau^2} + (\Omega_a^{\text{eff}})^2 \cdot \varphi &= 0, \\ (\Omega_a^{\text{eff}})^2 &= \Omega_a^2 - 2(N_y - N_x + h_u) \cdot \overline{\cos^2\chi} \\ &\quad - h_d \cdot \overline{\sin\chi} + h \cdot \overline{\cos\Omega\tau \cos\chi}, \end{aligned} \quad (5)$$

provided that $\Omega \approx \Omega_o$ and $\Omega_a \ll \Omega_o$ (which is valid in our case of elliptical particles of aspect ratio approximately 1). Ω_a and Ω_o are the characteristic frequencies of small amplitude 'acoustical' and 'optical' oscillations in SAF, respectively, and are given by $\Omega_a = \sqrt{(N_y - N_x + h_u) - (\gamma_y - \gamma_x)}$ and $\Omega_o = \sqrt{(N_y - N_x + h_u) + (\gamma_y + \gamma_x)}$. Under these conditions, the variation in φ can be regarded as 'slow' compared to the 'fast' oscillations in χ , in which case averaging the χ - and Ω -terms in equation 5 over one period is justified (represented by the bar). The $\lambda\Omega_o$ -term in eq. 4 is the parameter characterizing the dissipation of energy in the system. Its value is associated with the Landau-Lifshitz-Gilbert damping parameter.

Using Eqs. (4) and (5), the stability criteria for the ground states can be derived (see supplementary):

$$\frac{h_y}{4\Omega_o^2} \leq A_c \sqrt{1 - \frac{3A_c^2}{4} \sqrt{\left(\gamma_f + \frac{h_d \sin\chi_0}{2\Omega_o^2}\right)^2 + \lambda^2 \left(1 - \frac{A_c^2}{4}\right)}},$$

where A_c is the critical oscillation amplitude derived in the supplementary, $\gamma_f = (\Omega - \Omega_c)/\Omega_c$, with $\Omega_c = \sqrt{\Omega_o^2(1 - 3A_c^2/4)/(1 + 5A_c^2/4)}$. The above result takes into account that $|\gamma_f| \ll 1$.

Thus, in the presence of biasing field asymmetry, the stability regions for the two ground states split, and can fully separate such that microwave frequency-amplitude areas exist where only one states is stable, as illustrated in Fig. 3. If resonantly excited within these areas (shown in grey), the system switches into the given stable AP-state and remains in it, now off-resonance with the excitation. The separation of the minima in Fig. 3 is the

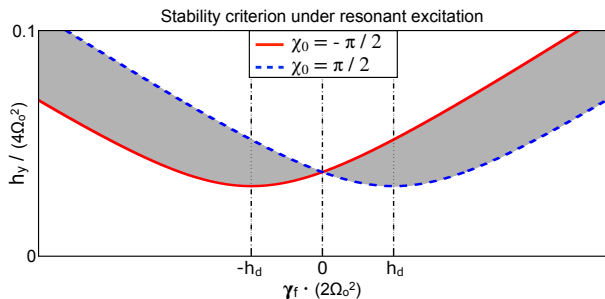


FIG. 3: (Color online) Stability diagram versus frequency-amplitude for the SFi ground states under resonant excitation. The curves separate the regions of stability and instability (below and above). The greyed out area shows the frequency-amplitude region where only one of the two states is stable, into which the system switches for given excitation. Ω_o is the optical center frequency (that of an ideal SAF), h_y the amplitude of the excitation, $\gamma_f = (\Omega - \Omega_c)/\Omega_c \Rightarrow \gamma_f \cdot 4\Omega_o^2 \propto \Omega - \Omega_c$, Ω the excitation frequency.

splitting in the optical eigen-mode of the system and is given by $\gamma_f = h_d/\Omega_o^2$.

The separation of the respective optical spin resonance frequencies is due to the difference in the effective biasing field acting on the individual layers. If the amplitude of the excitation is large enough and the frequency is chosen in resonance with a given ground state, switching into this state occurs, while the reverse switching is off-resonance and therefore disallowed energetically.

Interestingly, although the oscillation of the two macrospins is of optical type (out-of-phase), the switching occurs acoustically (in-phase rotation). The dipole-coupling is too strong for the moments to cross passed each other under the relatively weak microwave resonant fields used in this work. The switching trajectory is thus an in-phase rotation with superposed out-of-phase oscillations of smaller amplitude, with the energy effectively transferred from the pumped optical oscillations into a large-angle acoustical rotation. As a result, the expected fastest switching time is the half-period of the acoustical resonance frequency (corresponding to approximately 500 ps for our experimental geometry). For still faster resonant switching one would aim in the SFi-device design at maximizing the acoustical resonance frequency while maintaining a suitable size splitting in the optical resonance frequency; for example, by increasing the aspect ratio of the nanomagnets.

III. MACROSPIN SIMULATIONS

The macrospin simulations in this section solve the LLG equations for the system in the time domain, taking into account all the external and internal forces acting on the magnetic moments of the two layers, without the small-signal assumptions used in obtaining the analytical results. The simulation model is an extension of our previ-

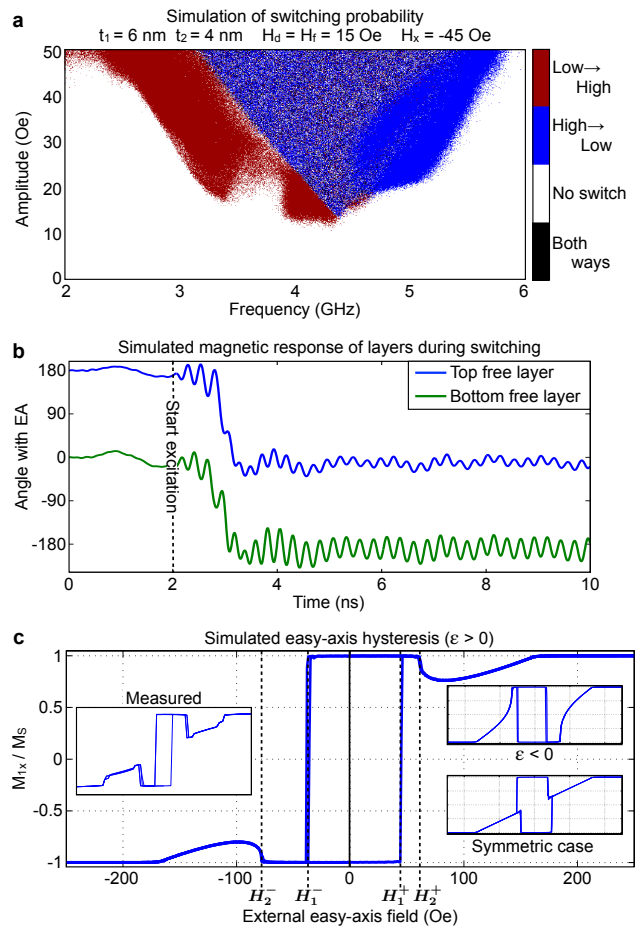


FIG. 4: (Color online) **a**, Switching probability map for the sample parameters given in the figure, showing a clear separation of the two AP states due to a biasing field and thickness asymmetry. **b**, Time trace of the two macrospins in the bilayer during a switching event, showing that the switching occurs via an in-phase rotation (acoustical mode), with superposed optical oscillations of smaller amplitude. **c**, Simulated easy-axis hysteresis for a sample with a thickness imbalance and biasing field asymmetry for $\epsilon > 0$ (main panel), corresponding to our typical experimental configuration (left inset), and for $\epsilon < 0$ (top-right inset). In contrast, an ideal, symmetric spin-flop bilayer shows a strictly anti-symmetric response (bottom-right inset; simulated).

ous work on the energetics of the SAF system^{16,28}. The magnetization vectors evolve in time driven by torques of the respective effective magnetic fields, with a suitably small time step of 5 ps. A thickness imbalance and fringing field are the two asymmetry parameters. The simulations include thermal agitation at $T = 300$ K.

In the case of no thickness imbalance, with the only asymmetry due to the unequal biasing fields on the individual free layers (from the reference layer built-in into the nanopillar), the numerically simulated switching behavior agrees well with that predicted analytically above. The optical resonance is clearly split, although the magnitude of the splitting is somewhat smaller.

A more pronounced resonance splitting is obtained by adding a thickness-imbalance to the magnetic asymmetry of the system. Figure 4a shows a typical simulated switching map. The area where switching occurs only in one direction is where only one ground state is dynamically stable. The general form of the stability regions simulated here for large-signal microwave excitation agrees well with the analytical results.

Figure 4b shows the real-time trace of the magnetization of the individual layers during a switching event. It is clear that the microwave-pumped oscillations are of optical nature but the switching itself is an "acoustical" in-phase rotation. The oscillations of the magnetization in the initial ground state under a resonant excitation of amplitude suitably large to produce switching are, in fact, smaller in the switched-to ground state since this state is now off-resonance with the microwave field. This effect of resonant state selection is a direct consequence of the magnetic asymmetry of SFi.

The full macrospin model further yields important insights into the quasistatic magneto-resistance properties of the junctions. Using Eq. 1 the quasistatic switching (H_1^\pm) and spin-flop fields (H_2^\pm) can be obtained and used for extracting the asymmetry parameters (individual layers' thicknesses and effective biasing fields) from the measured data. The interrelation between the thicknesses and fringing fields is (in notations of Fig. 4(c)):

$$\frac{H_i^\pm}{4\pi M_S} = \mp(-1)^i |\varepsilon| (N_y - N_x - \gamma_x) - h_f \pm \sqrt{\left(N_y - N_x + \gamma_x + h_u \pm (-1)^i \frac{\varepsilon}{|\varepsilon|} h_d\right)^2 - (1 - \varepsilon^2) \gamma_y^2},$$

$$|\varepsilon| \approx \frac{h_1^+ - h_1^- - h_2^+ + h_2^-}{4(N_y - N_x - \gamma_x)}, \quad h_f \approx \frac{-(h_1^+ + h_1^- + h_2^+ + h_2^-)}{4}.$$

Here $H_1^\pm = 4\pi M_S h_1^\pm$ is the field for which only one AP ground state becomes unstable and $H_2^\pm = 4\pi M_S h_2^\pm$ is the spin-flop field, at which both AP ground states become unstable. Note that the actual values of $H_{1,2}^\pm$ are slightly smaller than the analytical values due to thermal fluctuations.

IV. EXPERIMENTS

A. Samples

The samples used in the experiments were spin-flop type magnetic random access memory (TMRAM) cells with lateral dimensions of 450x375 and 420x350 nm, and elliptical in-plane shape. The stack consists of a magnetically soft SFi separated from a magnetically hard SAF reference layer by a thin Al-O tunnel barrier. The spin-flop bilayer is composed of two dipole coupled permalloy

ferromagnets (free layers) with thicknesses $t_1 \approx t_2 \approx 5$ nm (excluding the magnetically 'dead' layers at the film surfaces²⁹) separated by a ~ 1 nm thin TaN spacer, for which there is no interlayer exchange coupling, $J = 0$. Here t_1 and t_2 are the effective thicknesses of the bottom and top free layer, respectively. The SFM reference layer is nearly ideally flux-closed and is therefore essentially insensitive to external fields of strengths used in the experiments discussed in this paper. The samples used in this work had a weak fringing field from the reference layer acting on the two free layers. The fringing field originated predominantly from the top fixed layer. The resistance of the stack was ~ 1 k Ω , and the magnetoresistance $\sim 20\%$.

B. Measurement setup

In-plane quasi-static fields were applied using an external toroidal magnet³⁰. High-frequency fields were generated by contacting the on-chip integrated 50 Ω bit- and word-lines using surface probes with 0-40 GHz bandwidth. The bit- and word-lines were oriented at $\pm 45^\circ$ with respect to the the easy-axis of the stack in the so-called "toggling" configuration. A current through the bit- or word-line results in an in-plane magnetic field perpendicular to the line. In the results presented below, the high frequency excitation was applied using the word line only, which was electrically decoupled from the stack. The applied high-frequency fields were AC pulses of desired frequency ranging from 1 MHz to 10 GHz. The AC fields were generated using an Agilent E8247C PSG CW Signal Generator with a bandwidth of 250 kHz - 20 GHz. The wave-duration was controlled using an RF-switch driven by an Agilent 33250A AWG. The shortest possible pulse-length with this setup was 8 ns. The state of the sample was determined by measuring the resistance of the sample and thereby the relative orientation of the magnetization of the bottom free and top fixed layers. To separate the DC-signal from the RF-signal, a bias-tee was used.

C. Experimental results

The samples were SFi bilayers of approximately 5 nm thick Permalloy, separated by 1 nm thick TaN, integrated into approximately 350x400 nm in-plane elliptical nanopillars, also containing an Al-O read-out junction with a nominally flux-closed magnetic reference layer. The microwave excitation was applied using a closely spaced field-line making a 45° angle with the SFi easy axis. The ferromagnetic resonance frequencies were measured using transport spectroscopy, where the junction resistance versus frequency showed a maximum or a minimum for the low-resistance or high-resistance ground state, respectively. The resistance was measured while slowly sweeping the frequency of a continuous-wave ex-

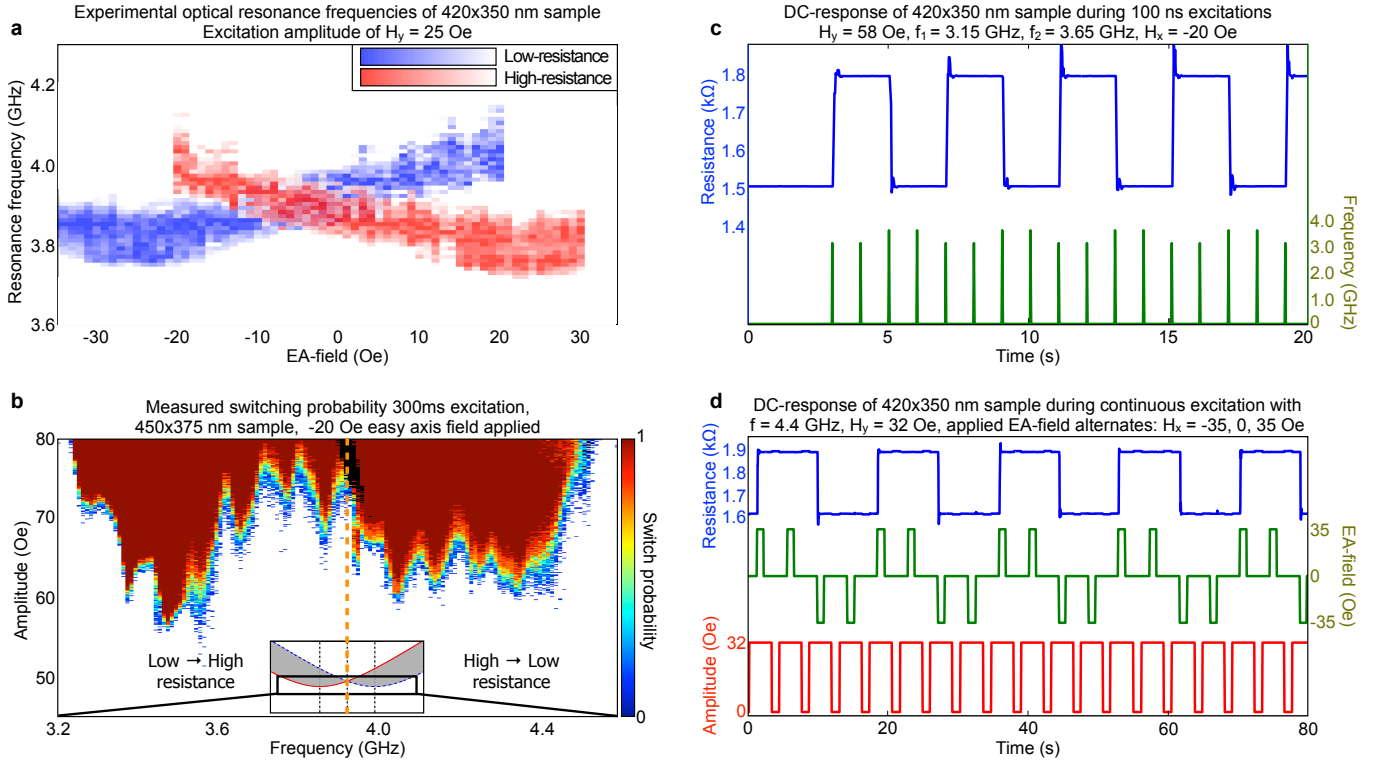


FIG. 5: (Color online) **a**, Measured resonance frequencies of a 420x350 nm spin-flop bilayer. The intensity map (red and blue for the two ground states) is normalized to the maximum oscillation amplitude for the given EA-field. **b**, Switching probability for the two ground states subject to 300 ms long excitation pulses with -20 Oe static EA-field applied. Black color denotes the frequency-amplitude points, for which switching in both directions occurred. The inset shows the section of the analytical switching map (Fig. 3) covered in the measurement. **c**, Real time resistance traces of a sample excited by short microwave pulses of alternating frequencies in resonance with the split optical mode, showing controlled resonant state selection. **d**, Resonant state selection using resonant microwave pumping of fixed frequency and alternating external EA-field, tuning the two ground states in and out of the optical spin resonance.

citation of fixed amplitude (typically 25 Oe). Figure 5a shows the measured resonance frequencies for the two AP ground states of a SFi with $M_0 < 0$, $H_1^m \approx 7$ Oe, $H_2^m \approx 3$ Oe and $t_1 - t_2 \approx 0.9$ nm (values deduced from quasistatic EA-hysteresis as shown in fig 4c). The splitting of the optical spin resonance at ≈ 4 GHz is in excellent agreement with the predicted behavior (Fig. 3).

Figure 5a shows the measured oscillation amplitude as a function of the excitation frequency and applied bias field. The amplitude is normalized with respect to the maximum value for each bias field. This diagram clearly shows that both field-controlled and frequency-controlled switching is possible.

Frequency-amplitude-switching maps were measured for both AP states (low- to high-resistance and high- to low-resistance) for different excitation pulse durations and static EA-fields. Figure 5b shows the switching maps for both AP states of the soft bilayer under 300 ms pulses of resonant excitation, with $H_x = -20$ Oe. Switching at frequencies lower than 3.9 GHz only occurs from the low- to high-resistance AP state ($f_{L \rightarrow H}$), while switching at above 3.9 GHz only occurs from the high- to low-resistance state ($f_{H \rightarrow L}$). Shortening the duration of the

excitation pulse requires a higher amplitude for switching the junction, at the same time leading to an increase in the error-rate likely due to a more non-linear and more non-uniform process for higher-amplitude pumping. Nevertheless, even for short excitations, the optical resonance is clearly split and amplitude-frequency regions exist where the switching is strictly one-directional. The weaker higher-order oscillations in the probability maps of Fig. 5b are due to secondary spin-wave excitations in our nanoparticles that are somewhat bigger than the true single-domain limit, which we also observe in our micromagnetic simulations as a small superposition on the well-defined macrospin behavior.

Figure 5c shows a realtime trace of the junction resistance during the application of a sequence of microwave pulses of 100 ns duration, of frequency alternating between the split optical spin-resonance peaks. A pair of pulses is sequentially applied at each frequency, demonstrating the strictly unidirectional character of resonant switching at a given frequency (for a given AP state of the SFi).

Figure 5d shows a realtime resistance trace (blue) under continuous microwave excitation of fixed frequency

near the centre of the optical resonance, with the EA-field of amplitude sufficient for tuning the two AP ground states in and out of the resonance. Between the EA-pulses the excitation is turned off shortly to confirm the state the sample is in (microwave amplitude shown in red; EA-field in green). The EA-field pulses were generated with an external electromagnet, so their shortest duration was 300 ms. The data show that the field-controlled resonance state selection is highly reliable.

Both measurements were repeated many times with the resulting error-rate smaller than 10^{-3} (1000 measurements were performed without any error). The effect is thus essentially deterministic for the sample and frequency-field parameters used, and still is expected to improve (e.g., in terms of speed) on scaling down the sample size.

V. CONCLUSIONS

We show how external microwave and static biasing fields can be used to tune the energetics and dynamics of a spin-flop system between symmetric and asymmetric be-

havior. We demonstrate controlled state selection in a synthetic ferrimagnet using a frequency modulated resonant microwave field or a uniform external biasing field. This effect is explained analytically using a small-signal analysis of the SFi spin dynamics, predicting a tunable splitting of the optical spin resonance, which is in good agreement with our numerical arbitrary signal-strength simulations. The effect is fast, robust, and offers a new way of magnetic switching of spin-flop nanodevices used in such large scale applications as magnetic random access memory.

Our analysis shows that the switching process is fast, $\sim 1/2f_a \sim 500$ ps, and proceeds through an in-phase (acoustical) spin rotation with superposed out-of-phase (optical) spin oscillations. Experimentally we demonstrate essentially error-free controlled switching down to 100 ns in pulse duration of the resonant microwave excitation. Smaller, more single-domain-like samples (sub-100 nm range), with optimized magnetic asymmetry and increased aspect ratio are expected to show significantly faster resonant switching due to reduced generation of unwanted spin-wave modes and higher acoustical frequencies.

-
- * Corresponding author: vk@kth.se
- ¹ M. N. Baibich, J. M. Broto, A. Fert, F. Nguyen Van Dau, F. Petroff, P. Etienne, G. Creuzet, A. Friederich, and J. Chazelas. *Phys. Rev. Lett.*, **61**, 2472, (1988).
 - ² G. Binasch, P. Grünberg, F. Saurenbach, and W. Zinn. *Phys. Rev. B*, **39**, 4828, (1989).
 - ³ M. Julliere. *Phys. Lett. A*, **54**, 225, (1975).
 - ⁴ J. S. Moodera, Lisa R. Kinder, Terrilyn M. Wong, and R. Meservey. *Phys. Rev. Lett.*, **74**, 3273, (1995).
 - ⁵ B. Dieny, V. S. Speriosu, S. S. P. Parkin, B. A. Gurney, D. R. Wilhoit, and D. Mauri. *Phys. Rev. B*, **43**, 12970, (1991).
 - ⁶ Th. Gerrits, H. A. M. van den Berg, J. Hohlfeld, L. Bar, and Th. Rasing. *Nature*, **418**, 509, (2002).
 - ⁷ Anders Bergman, Björn Skubic, Johan Hellsvik, Lars Nordström, Anna Delin, and Olle Eriksson. *Phys. Rev. B*, **83**, 224429, (2011).
 - ⁸ C. H. Back, R. Allenspach, W. Weber, S. S. P. Parkin, D. Weller, E. L. Garwin, and H. C. Siegmann. *Science*, **285**, 864, (1999).
 - ⁹ S. Kaka and S. E. Russek. *Appl. Phys. Lett.*, **80**, 2958, (2002).
 - ¹⁰ J. C. Slonczewski. *J. Magn. Magn. Mater.*, **159**, L1, (1996).
 - ¹¹ M. C. Wu, A. Aziz, D. Morecroft, M. G. Blamire, M. C. Hickey, M. Ali, G. Burnell, and B. J. Hickey. *Appl. Phys. Lett.*, **92**, 142501, (2008).
 - ¹² E. B. Myers, D. C. Ralph, J. A. Katine, R. N. Louie, and R. A. Buhrman. *Science*, **285**, 867, (1999).
 - ¹³ A. Brataas, A. D. Kent, and H. Ohno. *Nature Mater.*, **11**, 372, (2012).
 - ¹⁴ B.N. Engel, J. Akerman, B. Butcher, R.W. Dave, M. DeHerrera, M. Durlam, G. Grynkewich, J. Janesky, S.V. Pietambaram, N.D. Rizzo, J.M. Slaughter, K. Smith, J.J. Sun, and S. Tehrani. *IEEE Trans. Magn.*, **41**, 132, (2005).
 - ¹⁵ H. T. Nembach, C. Bayer, H. Schultheiss, M. C. Weber, P. Martin Pimentel, P. A. Beck, B. Leven, and B. Hillebrands. *Appl. Phys. Lett.*, **87**, 142503, (2005).
 - ¹⁶ D. C. Worledge. *Appl. Phys. Lett.*, **84**, 4559, (2004).
 - ¹⁷ A. V. Kimel, B. A. Ivanov, R. V. Pisarev, P. A. Usachev, A. Kirilyuk, and Th. Rasing. *Nature Phys.*, **5**, 727, (2009).
 - ¹⁸ Y.-T. Cui, J. C. Sankey, C. Wang, K. V. Thadani, Z.-P. Li, R. A. Buhrman, and D. C. Ralph. *Phys. Rev. B*, **77**, 214440, (2008).
 - ¹⁹ T. Moriyama, R. Cao, John Q. Xiao, J. Lu, X. R. Wang, Q. Wen, and H. W. Zhang. *Appl. Phys. Lett.*, **90**, 152503, (2007).
 - ²⁰ S.S. Cherepov, V. Korenivski, and D.C. Worledge. *IEEE Trans. Magn.*, **46**, 2112, (2010).
 - ²¹ V. Korenivski and D. C. Worledge. *Appl. Phys. Lett.*, **86**, 252506, (2005).
 - ²² A. Konovalenko, E. Lindgren, S. S. Cherepov, V. Korenivski, and D. C. Worledge. *Phys. Rev. B*, **80**, 144425, (2009).
 - ²³ S. S. Cherepov, B. C. Koop, Yu. I. Dzhezherya, D. C. Worledge, and V. Korenivski. *Phys. Rev. Lett.*, **107**, 077202, (2011).
 - ²⁴ D. W. Abraham and D. C. Worledge. *Appl. Phys. Lett.*, **88**, 262505, (2006).
 - ²⁵ D. C. Worledge. *Appl. Phys. Lett.*, **84**, 2847, (2004).
 - ²⁶ S.-Y. Wang and H. Fujiwara. *J. Appl. Phys.*, **98**, 024510, (2005).
 - ²⁷ A. M. Kosevich, B. A. Ivanov, and A. S. Kovalev. *Physics Reports*, **194**, 117, (1990).
 - ²⁸ W. J. Gallagher and S. S. P. Parkin. *IBM J. Res. Dev.*, **50**, 5, (2006).
 - ²⁹ D. W. Abraham, P. L. Trouilloud, and D. C. Worledge. *IBM J. Res. Dev.*, **50**, 55, (2006).

- ³⁰ M. C. Gaidis, E. J. O'Sullivan, J. J. Nowak, Y. Lu, S. Kanakasabapathy, P. L. Trouilloud, D. C. Worledge, S. Assefa, K. R. Milkove, G. P. Wright, and W. J. Gallagher. IBM J. Res. Dev., **50**, 41, (2006).